Chemical Engineering Journal 158 (2010) 25–31

Contents lists available at ScienceDirect

Chemical Engineering Journal

journal homepage: www.elsevier.com/locate/cej

Measuring gas hydrate formation and exchange with CO_2 in Bentheim sandstone using MRI tomography

G. Ersland [a,*], J. Husebø [a], A. Graue [a], B.A. Baldwin [b], J. Howard [c], J. Stevens [c]

[a] University of Bergen, Bergen, Norway
[b] Green Country Petrophysics LLC, Dewey, OK, USA
[c] ConocoPhillips, Bartlesville, OK, USA

ARTICLE INFO

Article history:
Received 7 May 2008
Received in revised form 18 December 2008
Accepted 19 December 2008

Keywords:
MRI tomography
Gas hydrate
CO_2 sequestration
IDL programming

ABSTRACT

Formation of methane hydrate in Bentheim sandstone was monitored *in situ* with magnetic resonance imaging (MRI). Sequestration of CO_2 in hydrate accumulations was achieved by exposing the hydrate to liquid CO_2. The spontaneous exchange of methane with CO_2 within the hydrate structure was monitored by MRI. The process of CO_2–CH_4 exchange in hydrates without the addition of heat or melting hydrate has the potential as a viable strategy for thermodynamically stable long term CO_2-sequestration, with the added benefit of associated natural gas production. The MRI proved to give excellent information about the spatial distribution of the hydrate growth, the rate of the hydrate formation and the rate of the CO_2–CH_4 exchange. A standardized and reliable data analysis software package was developed to handle the huge amount of MRI-generated data.

1. Introduction

Natural gas hydrate is a chemical compound formed under high-pressure and low temperature conditions. This compound consists of water molecules interconnected through hydrogen bonds creating an open structural lattice with the ability to encage natural gas molecules. There is an abundance of known natural gas hydrate reservoirs around the world, with an estimated energy potential that exceeds that of conventional oil, gas and coal by a factor of two [1]. To help bring this potential resource to production, an improved understanding of hydrate formation and reformation kinetics is needed. Although limited information is available on the field scale, measurements on sediment samples may clarify characteristics of gas hydrate reservoirs and technical issues related to natural gas production from them. This study is part of an ongoing effort to help determine if gas hydrates may become a viable energy source for the future.

There are essentially two different approaches to produce natural gas from hydrate reservoirs. Either bring the hydrate out of its thermodynamic stability zone or expose the hydrate to a substance that will form a more stable hydrate structure, forcing an *in situ* exchange of the trapped molecules in the structural lattice. One of the problems with bringing hydrates out of its thermodynamic stability zone is that the dissociation of hydrate frees the hydrate bound water as well as destabilizes the reservoir sediments. The excess water causes production problems while the lowered reservoir stabilization increases the risk for large-scale collapses, which might have catastrophic consequences. These potential problems can be avoided by exposing hydrate to a thermodynamically preferred hydrate former. This may induce an *in situ* exchange that will increase the stability of the reservoir sediments as well as maintain hydrates in the solid state.

In the work presented here methane hydrate was formed in whole and fractured Bentheim cores, all with 22–23% porosity. The absolute permeability was measured to 1.1 Darcy. The sandstone was partially saturated with water and pressurized to 1200 psig using methane. The core was then cooled to methane hydrate stable conditions. After the hydrate formation, the core was exposed to liquid CO_2 in order to initiate a CH_4–CO_2 exchange. Magnetic resonance imaging (MRI) was used to monitor the formation of methane hydrate as well as transforms the reformation of CO_2–hydrate. When hydrates form, water goes from liquid to solid state, this significantly reduces the relaxation time of the protons making MRI a powerful tool for monitoring this process. MRI also gives quantitative information of the CH_4–CO_2 exchange rate.

An in-house build program was developed to analyze the huge amount of 3D-data generated by the MRI. This software was called ROI (region of interest), it has a graphical user interface (GUI) and is developed using the IDL platform (http://www.ittvis.com/idl/). The ROI software is able to monitor hydrate formation, dissociation and reformation versus time and is able to perform noise processing algorithms to improve analysis of the experimental data.

* Corresponding author. Tel.: +47 55 58 28 68; fax: +47 55 58 94 40.
E-mail address: geir.ersland@ift.uib.no (G. Ersland).

1385-8947/$ – see front matter © 2009 Published by Elsevier B.V.
doi:10.1016/j.cej.2008.12.028

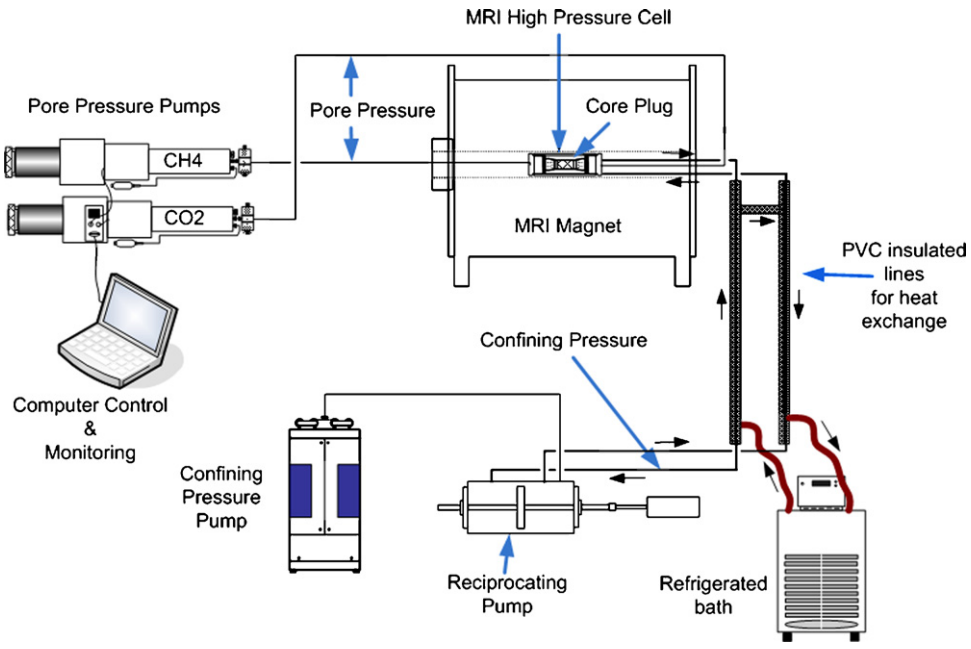

Fig. 1. Experimental apparatus.

2. Magnetic resonance imaging of gas hydrates

2.1. Experimental

A schematic of the experimental apparatus is shown in Fig. 1. The system consists of the core sample, a core holder to maintain the sample at high-pressure and low temperature, a high-pressure control system (overburden), inlet and outlet pumps, and the MRI to monitor the distribution of water, hydrate and methane. Fluorinert (FC-40) was used as both the confining fluid and the temperature control medium. Fluorinert is a fluorocarbon and contains no hydrogen atoms, thus it is not imaged, and its low dielectric properties minimize radio frequency (RF) losses. This fluid was maintained at the desired pressure while circulated through the cooling system and cell by use of a recirculation pump. The strong magnetic field associated with MRI required that all temperature and pump controllers were positioned several meters away from the magnet. The high-pressure coolant lines were centered inside a low pressure PVC jacket with its own temperature-controlled circulating fluid to maximize heat exchange prior to the Fluorinert enters the MRI cell. This feature made the temperature control accurate to ±0.1 °C during weeks of operation.

An illustration and a cross-sectional diagram of the pressure cell used in the MRI setup are shown in Fig. 2. This is a Hassler-type core holder designed and constructed under the direction of Temco Inc©, Tulsa, OK. This high-pressure cell is constructed from materials that are compatible with the strong magnetic and RF fields generated by the MRI. The housing is made with alternating-direction spiral wounds-glass fibers embedded in a catalyzed resin for strength. This housing is strong enough to handle the pressure of the experiments, however because the fiber glass housing has micro porosity, an inner *Aflas*® liner is used between the confining area and the outer wall of the cell to prevent leakage. The end caps are made from titanium and are held in place by non-magnetic cobalt screws that threads through the housing into the end cap. The end caps contains two holes acting as system line pass-through, these are sealed around the system lines using o-rings. The maximum working pressure is 6000 psi (41.4 MPa) and maximum working temperature is 200 °F (93 °C). The confining fluid is connected to two lines on one of the end caps. One of the confining lines passes through to the other side of the confining volume and allows the fluid to circulate.

The end pieces directly connected to the core are constructed from *Polyetheretherketone* (*PEEK*™). They are assembled with the core using two *Polyoxymethylene* (*POM*) end spacers on the core ends and two layers of *Teflon*® shrink tubing around the core. The seal is provided by an o-ring milled into the end piece. The pass through on the cell end caps stabilizes the end piece and helps to hold the core and shrink tubing in place.

The MRI is a Unity/Inova-Imaging 85/310 spectrometer made by Varian Inc, Palo Alto, CA. It has a resonance frequency of 85.7 MHz (approximately 2 T). The RF coil was a 13.3 cm (5.25″) ID 85 MHz ^{1}H Quadrature Bird Cage Coil with an RF window 27.9 cm (11.0″) long. The spatial resolution used is in the sub-millimeter scale. All the images were acquired with standard spin-echo sequences.

Because the water wetted the pore surface and interacted with the mineral surface, the T2* relaxation was short, <150 ms, while T1 was typically 1–2 s. To obtain reasonable signal intensity from the 2D and 3D spin-echo images the echo time was set to be short, typically <3 ms, while the recovery time, was between 2 and 4 s. The two types of data acquisition used for numerical analysis of the following experiments are one dimensional profiles and three dimensional images. The one dimensional profiles are a series of points (typical 256 floating points)[1] along the MRI field of view and give a one dimensional illustration of the hydrogen distribution along any of the three axes (usually the profiles were taken along the length of the core). Profiles are good for quick analysis such as saturation distribution and MRI acquisition of rapid experimental processes when three dimensional images take too long to acquire. An MRI profile is generally taken within less than a minute. The three dimensional images are $32 \times 32 \times 128$ floating point arrays that represent the hydrogen distribution in three dimensions. This is a great way to illustrate fluid-phase distribution in the core. Since the resolution of the MRI is in the sub-millimeter scale, each voxel within the three dimensional image represents pore clusters rather than single pores. Three dimensional images

[1] A 32 bit number that can be any 8 significant digit value within the -10^{38}–10^{38} range.

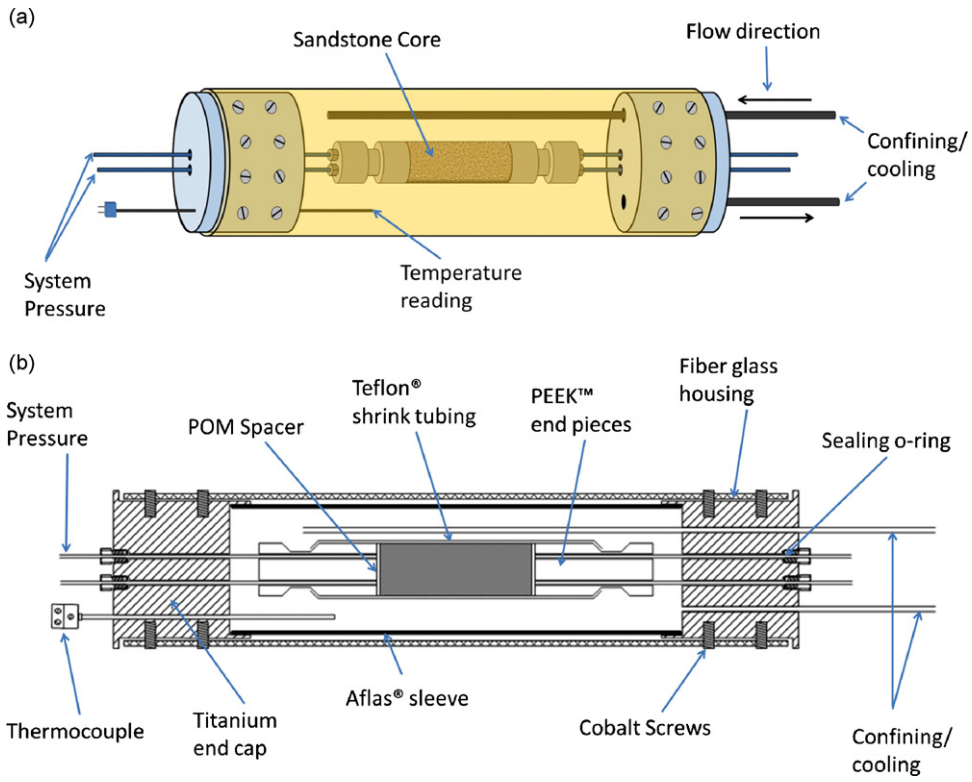

Fig. 2. (a) Illustration of MRI high-pressure cell. (b) Cross-sectional diagram of MRI high-pressure cell.

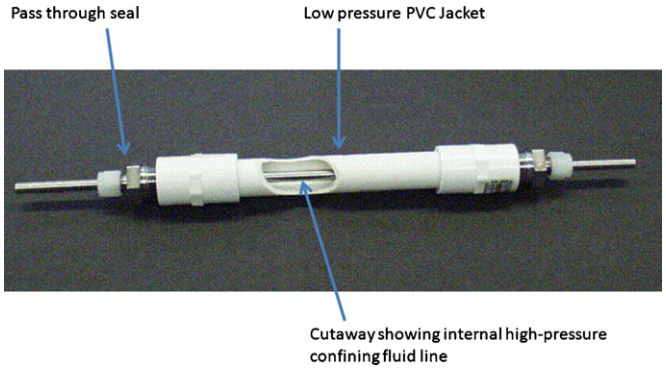

Fig. 3. Cut away model of the heat exchange system for the confining line.

take between 1 and 9 h to acquire, depending on the desired signal-to-noise ratio.

A heat exchange system was created in order to minimize the heat loss before the cooled fluorinert reached the pressure cell. This heat exchange system consists of two several-meter long lengths of high-pressure stainless steel tubing centered and sealed inside low pressure PVC pipe. A cutaway of this is shown in Fig. 3. In use, these lines were covered with insulation to further minimize heat loss and prevent condensation on the lines. The void between the PVC line and the high-pressure confining line was filled with antifreeze which was temperature controlled and circulated using a *Thermo Neslab RTE-17* refrigerated bath.

2.2. Monitoring hydrate growth in sandstone core plugs

The MRI detects gas hydrate as a large drop in intensity between images of liquid water and solid hydrate. Hydrate formation is measured as the loss of MRI intensity as the liquid water converts to solid hydrate. Hydrogen in the solid hydrate has a short relaxation time and is not detected by MRI (no signal above the background level). In contrast, the hydrate precursors, water and methane, produce intense MRI images.

Two different methods were used to establish uniform water saturation in the partially saturated whole core samples. The first approach started with a fully water-saturated core assembled in the core holder. Uniform saturation distributions were established by pulling vacuum from one end. Average MRI intensity was used to measure the saturation as function of time during desaturation. The evacuation valve was closed and methane was introduced to the system when reaching the predefined water saturation. The idea behind this approach was to establish uniform saturations of methane and water without introducing air. Unfortunately, a problem emerged for some experiments when the system temperature was lowered; condensation of water vapor formed hydrate and plugged flow lines. To avoid this problem the saturation was established outside the cell in later experiments. This way the flow lines were kept dry. When assembled, several PV's of methane were injected through the core to minimize the amount of air in the system. Hydrate formed without problems for both techniques, with no distinct difference in induction time or formation rate, but the latter method eliminated hydrate formation in the lines.

The gas hydrate formation starts spontaneously after an induction time between 0 and 35 h as the system was cooled and the temperature reached the gas hydrate thermodynamic zone. The Induction time seemed to decrease with salinity and saturation, but this is not known to any scientific precision. Hydrate formation was detected as a sudden consumption of methane and a corresponding drop in MRI intensity. Methane consumption from pump volume logs and loss of MRI intensity served as independent measurements of hydrate formation as function of time. The system temperature was never allowed below 3.6 °C to ensure only three phases were present at any time (methane gas, liquid water and

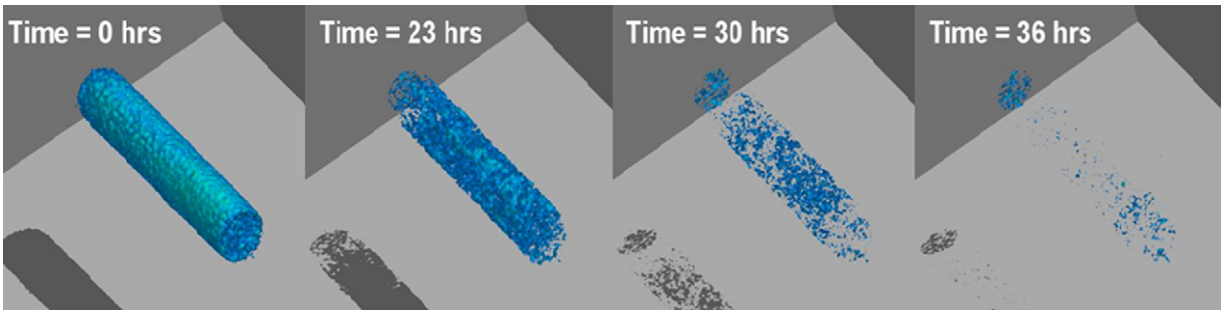

Fig. 4. Hydrate formation in whole core [3].

solid methane hydrate) i.e. no ice was formed. A visualization of hydrate formation is shown in Fig. 4 for a whole core with 50% initial brine saturation. The brine used was deionized water with 0.1 wt% NaCl added. The first image was obtained at the start of cooling, with water and methane in the core, and water as the predominant signal source. Images 2–4 show uniform growth pattern throughout the core. The rate of hydrate formation declined after an initial rapid growth of 30 h, but continued for over 90 days. A more piston-like formation pattern was observed for higher initial saturations. As can be seen from the 3D-visualization very little free water was left behind (<5%), however, for higher salinities (3–5 wt% NaCl), more of the water was not converted. This is may be explained as the result of increased salt concentration in the residual water preventing complete formation. High salinity is known to restrict hydrate formation [1,2]. Other factors that is likely to control growth pattern in sediment samples may include sediment mineralogy and texture, gas composition, and whether hydrate forms from free or dissolved gas.

2.3. Monitoring CO_2–CH_4 exchange

To investigate CO_2–CH_4 exchange a core sample was assembled consisting of two half cylindrical cores separated with a 4 mm thick spacer (see Fig. 5). The high-molecular weight polyethylene spacer was machined to have a series of rectangular holes in the vertical support to allow easy transport of water and gas through the frame. This centered spacing was constructed to serve two purposes: Increase the surface area for CO_2 to enter the core during exchange, and create an open volume to measure MRI Intensities of the CO_2–CH_4 mixture avoiding signal contribution from liquid water. This way, the MRI intensity was a direct measure of the methane concentration within the spacer as function of time, that is, a measure of methane diffusing from free gas in the pore space and methane produced from gas hydrates. It was experimentally verified that the normalized MRI intensity (1 = pure methane) was a direct measure of the molar methane concentration in the fracture. The linear relationship was proved within a few per cent discrepancy at experimental conditions.

Fig. 6 shows a series of MRI images collected from the core with spacer. The first image (A) was acquired after the system (core, spacer and lines) was evacuated and pressurized to 1200 psig with pure methane. This visualization reveals the MRI signal intensity from methane in the spacer. At this time both spacer and the two core halves was filled with methane, but the signal from the matrix was low and was set to be below the noise threshold. A total of 9 h continuous recordings (16 signal averages) were needed to obtain a reasonable signal-to-noise ratio from the methane in the pores. The second image (B) shows mostly water in the core and was obtained after injecting 12 cc of brine (5 wt% NaCl) into the spacer and allow it to imbibe. The signal in the spacer was still from the methane as all the water imbibed into the two core halves. After establishing fairly uniform water saturations (56% average) the system was cooled and hydrates started forming after an induction time of 27 h after reaching 4 °C. Image (C) shows hydrate forming from the top in the left-hand core half progressing downwards. The last image (D) was obtained after 135 h showing most of the water converted hydrate and a region of residual water in the rightmost front.

Diffusion processes appeared to be the dominant driving mechanism in supplying CO_2 to the methane hydrate reaction sites and the concomitant increase of methane in the fracture. The exchange process continued over several weeks. When methane production ceased, the spacer was again flushed with CO_2 to accelerate the reaction by supplying fresh and pure liquid CO_2 to the system. Fig. 7 shows a series of MRI images as function of time after the flush. As the system was closed, CO_2 was allowed to diffuse into the two core halves and methane was allowed to be produced back into the spacer. The first image obtained after the flush (A) reveal no signal in the spacer, indicating that most of, if not all, the methane was displaced by CO_2. This was confirmed by GC analysis (gas chromatography) of the effluent sample. The second image (B) was acquired 45 h after the flush, at this time the MRI signal reappear in

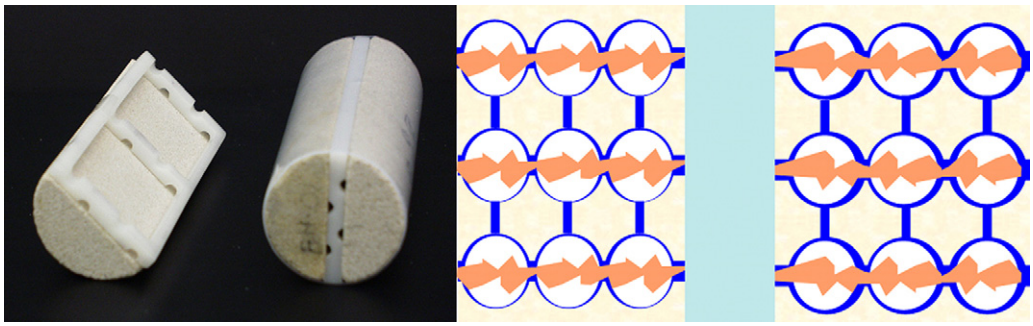

Fig. 5. Left: core with spacer. Right: schematic of the system with the spacer (middle green) and possible pore-filling after hydrate formation. Blue is liquid water, white is methane hydrate and orange is methane gas.

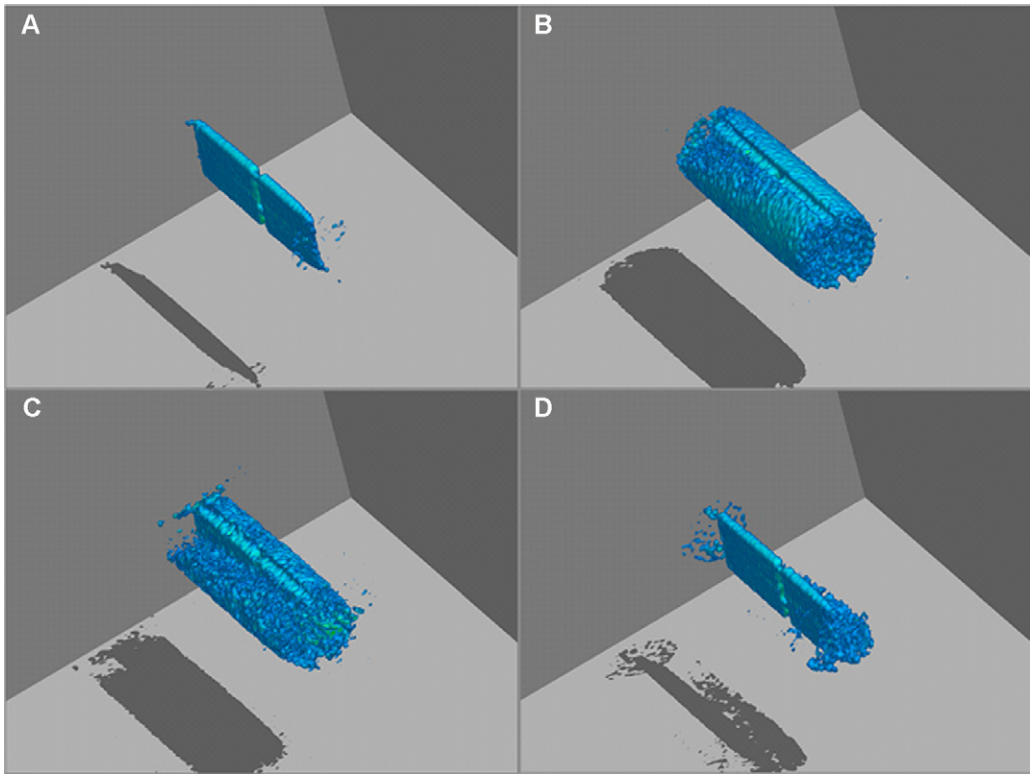

Fig. 6. (A) Methane in spacer (B) core and spacer after water injection and imbibition (C) hydrate formation starting in the left core half (D) methane in fracture and residual water in the core.

the fracture. (C) and (D) show successive images, obtained after 195 and 315 h respectively, as methane continuously was produced into the spacer. To increase the signal-to-noise ratio averaging was used in all images. Run time for each image was about 1 h (two signal averages). Increased signal averaging was performed at late times after the flush (16 signal averages). The effect of increased signal averaging can be seen in image (D) as much of the random noise in image (C) is eliminated.

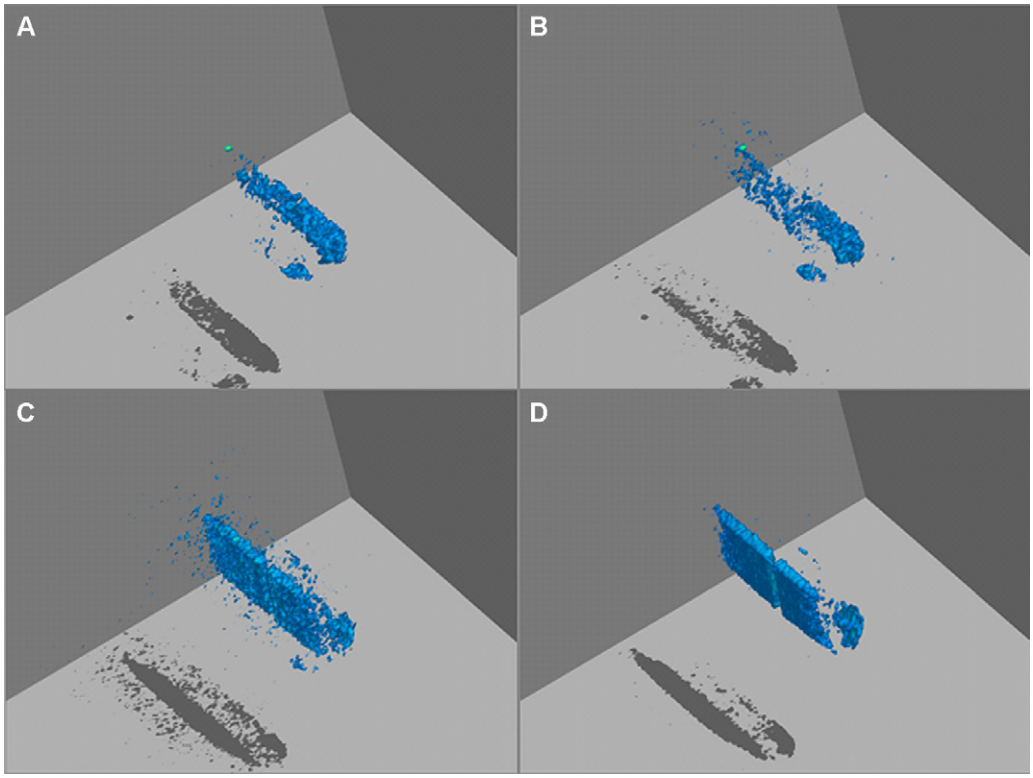

Fig. 7. (A) CO_2 in spacer (B) methane in spacer (42 h after CO_2 injection) (C) methane in spacer (195 h after CO_2 injection) (D) methane in spacer (315 h after CO_2 injection).

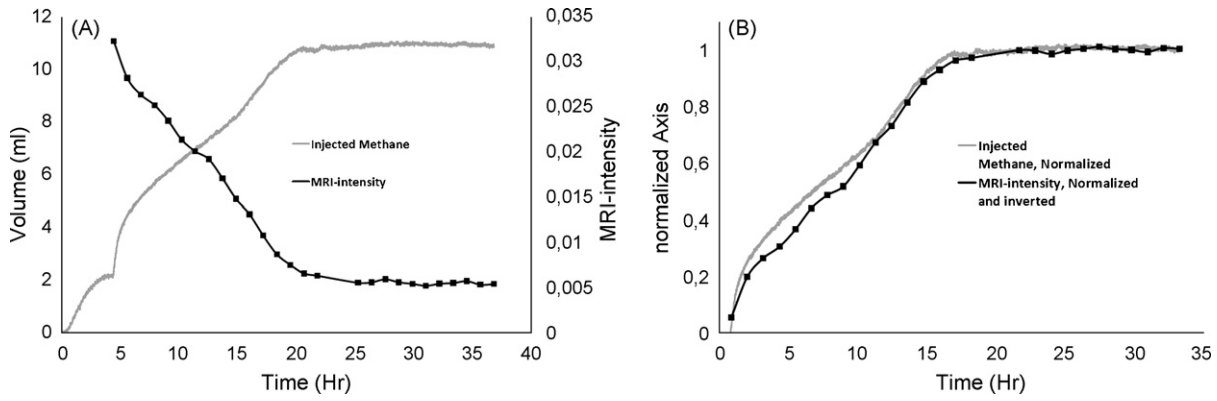

Fig. 8. Correlation between consumed methane and MRI-intensity [4].

The MRI images did not detect any significant increase in signal in the hydrate saturated cores that would indicate the presence of free water during the carbon dioxide replacement. MRI intensity in the core remained constant or decreased below the baseline value after the completion of methane hydrate formation. The spatial resolution of the MRI measurement does not rule out the possibility of small-scale dissociation and reformation of the hydrate phases. There is now precise model on the conversion mechanism for the reformation of methane hydrate over to CO_2. One hypothesis for the conversion mechanism is that liquid CO_2 molecules approaching the methane hydrate surface induce a microscopic dissociation of the outer hydrate layer. The released liquid-like molecule then subsequently forms hydrate with CO_2. Within the simplified two phase exchange model described in Kvamme et al. [3], a diffusivity coefficient of 1.7×10^{-9} m^2/s predicted similar production rates as observed in these experiments. This value closely reassembled diffusivity of CO_2 in aqueous solution (1.56×10^{-9} m^2/s at 30 °C).

Although methane is produced by both diffusion from free methane in the pore space and by CO_2–CH_4 exchange followed by diffusion, the contribution from each process cannot be measured in the MRI. For this reason a separate experiment measuring diffusion only was conducted using the same approach but excluding cooling to prevent hydrate formation. The contribution from diffusion of free methane in a core saturated with 50% methane and 50% water was found to be below 2/7 of the total amount of methane produced when hydrates was formed before introducing CO_2. This result, along with calculations based on MRI intensities only, unequally states that the methane produced by far exceeds the maximum amount of free methane available in the open pore space at the beginning of the experiment.

Another observation is the apparent absence of large-scale melting of hydrates during the CO_2–CH_4 exchange. Melting of hydrates would have been easily detected as a major intensity increase caused by the release of free water in the core. In fact, more of the residual water after hydrate formation (see Fig. 7A) seems to be converted after introducing CO_2 (see Fig. 7D). This apparent absence of large-scale melting may have significant implications for commercial aspects of this proposed exploitation strategy.

2.4. ROI program and analysis

The 3D visualizations of the MRI images acquired during the experiments provide excellent qualitative information of both hydrate formation and reformation. However, signal analysis was needed in order to quantify time dependant patterns, directional noise as well as singularities on a millimeter scale. This need was met by in-house built software called ROI developed on the IDL platform. The main focus of this program is to do real-time in-situ analysis of the hydrate formation and the CH_4–CO_2 exchange. The program also reduces uncertainties by identifying anomaly patterns and singularities in the MRI data.

The ROI program is essentially a graphical user interface that lets the user visualize the MRI data and choose a three dimensional region of interest. An algorithm can then be applied to this region. This algorithm performs a series of calculations all specifically designed to identify certain occurrences within the MRI data. The program then presents an array of results that give grounds for a more quantitative analysis of the MRI date obtained from the experiment.

Fig. 8 (left) shows the rate of hydrate formation as a decline in MRI intensity and consumed methane as a function of time in a whole core plug. The first 4–5 h the methane injected represent the volume needed to maintain the system pressure at 1200 psig during cooling. When cooled, hydrate formation can be identified as an abrupt increase of consumed methane and a corresponding drop in the MRI Intensity. A clear correlation between the two measurements is shown in the right plot in Fig. 8. A simple plot of the water distribution in the core based on MRI Intensities is shown in Fig. 9.

The additional laboratory equipment surrounding the MRI causes a series of challenges with the analysis of the acquired MRI images. Any electromagnetic noise may cause interference with the magnetic field of the MRI or the electronics generating the three dimensional images. This can result in both directional and non-directional noise in the image both of witch ROI is capable of detecting and circumventing with great success.

Fig. 10 shows the methane build-up in the spacer as function of time after liquid CO_2 is flushed trough the spacer. The reproducibility between experiments is excellent. After methane production

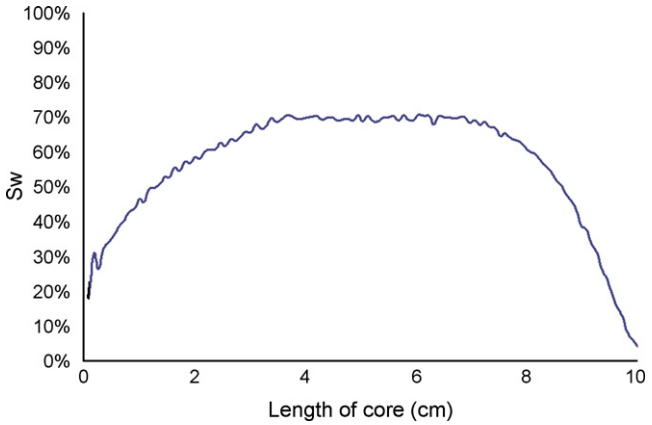

Fig. 9. Water distribution in core as function of length.

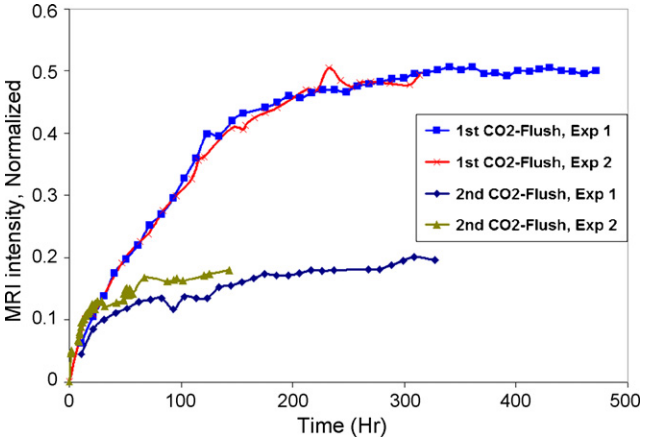

Fig. 10. Methane production shown by MRI-intensity build-up in spacer for two similar experiments. MRI-intensity is normalized against 100% methane [5].

ceased, a second flush of CO_2 through the spacer was performed and even more methane was produced into the spacer.

3. Conclusions

MRI was found to provide excellent images of high resolution that distinguished between the hydrate and its liquid/gas precursors and allowed for dynamic, spatial imaging of the formation and reformation of hydrates in the porous sandstone.

Exposing the hydrate saturated core to liquid CO_2 initiated a spontaneous in-situ exchange between methane and carbon dioxide. This conversion occurred without any measurable hydrate dissociation.

The ROI program was proven to be an efficient tool when performing quantitative analysis of the MRI data acquired during the experiments. The use of a standardized tool makes it easier to compare results and the efficiency of the noise-handling algorithm lowered the experimental uncertainties and was helpful in showing reproducible results between experiments.

References

[1] E.D. Sloan, Clathrate hydrates of natural gases, in: Revised and Expanded, Second edition, Marcel Dekker, New York, 1998, p. 21.
[2] L.G. Tang, G. Li, Y.M. Hao, R. Xiao, C. Huang, Ss. Fan, Z.P. Feng, Effects of salt on the formation of gas hydrate in porous media, in: Proceedings of the 5th international Conference Gas Hydrates, Trondheim, Norway, June 12–16, 2005.
[3] B. Kvamme, A. Graue, T. Kuznetsova, T. Buanes, G. Ersland, Energy from natural gas hydrate combined with reservoir storage of CO_2, WSEAS Transactions on Environment and Development 2 (6) (2006), ISSN: 1790-5079.
[4] J. Husebø, B. Kvamme, A. Graue, In-situ hydrate formation and reformation kinetics measured by magnetic resonance imaging, WSEAS Transactions on Systems and Control 2 (January) (2007), 2007, ISSN: 1991-8763.
[5] A. Graue, B. Kvamme, B.A. Baldwin, J. Stevens, J. Howard, G. Ersland, J. Husebø, D.R. Zornes, Magnetic resonance imaging of methane–carbon dioxide hydrate reactions in sandstone pores, SPE (2006), 102915.